International Journal of Multiphase Flow 35 (2009) 485–497

Contents lists available at ScienceDirect

International Journal of Multiphase Flow

journal homepage: www.elsevier.com/locate/ijmulflow

Liquid/liquid dispersion in a chaotic advection flow

Charbel Habchi [a,b], Thierry Lemenand [a], Dominique Della Valle [a], Hassan Peerhossaini [a,*]

[a] Thermofluids, Complex Flows and Energy Research Group, Laboratoire de Thermocinétique de Nantes, CNRS UMR 6607, École Polytechnique – Université de Nantes, rue Christian Pauc, B.P. 50609, 44306 Nantes, France
[b] Agence de l'Environnement et de la Maîtrise de l'Énergie (ADEME), 20 avenue du Grésillé, B.P. 90406, 49004 Angers, France

ARTICLE INFO

Article history:
Received 12 September 2008
Received in revised form 10 February 2009
Accepted 22 February 2009
Available online 12 March 2009

Keywords:
Chaotic advection
Liquid/liquid dispersion
Drop size distribution
Multifunctional heat exchanger

ABSTRACT

Mixing by chaotic advection in a twisted-pipe flow is used here to investigate the efficiency of this flow in the liquid/liquid dispersion process. This study focuses on water/oil dispersions produced by continuous water injection into a main oil flow, for small Dean numbers. The drop sizes obtained with the chaotic-advection twisted-pipe flow are compared with those in a straight pipe and a helically coiled flow for the same conditions. It is found that the resulting dispersions are finer and more mono-dispersed in the chaotic advection flow. These results are compared with the theoretical maximum diameter d_{max} determined by the Grace theory in which the viscous stress controls the breakup phenomena. For this purpose, the kinematic field is computed from the theoretical formulae for Dean flow. The strain rate fields in the pipe cross-section are then analytically computed and used to predict the maximum drop diameter. The theoretical values are identical for the three configurations (straight, helically coiled, and twisted pipe) up to a critical Dean number, where the secondary flow becomes significant. Beyond this value, the shear stress is enhanced in the twisted-pipe flow compared with the straight-pipe flow, and the predicted drop diameters are smaller. An interpretation of the higher dispersive performance of the chaotic flow is provided by the Lagrangian trajectories of the particles.

© 2009 Elsevier Ltd. All rights reserved.

1. Introduction

The advantages offered by a chaotic-advection twisted pipe-flow used as a mixer and/or heat exchanger have been established in previous studies (Aref, 1984; Jones et al., 1989; Acharya et al., 1992; Peerhossaini et al., 1993; Castelain et al., 1997; Mokrani et al., 1998a,b; Le Guer et al., 2001; Lemenand and Peerhossaini, 2002) when compared with a straight pipe or helically coiled pipe. The geometric perturbation of the twisted-pipe configuration generates three-dimensional chaotic trajectories in the secondary Dean flow induced by curvature effects. The Dean number characterizes the ratio between the viscous forces and the centrifugal forces, and is defined as

$$De = \frac{W^2 a^3}{R\nu^2} \tag{1}$$

where a is the tube inner radius and R the bend curvature radius.

Chaotic advection in such geometries produces efficient macro-mixing and heat transfer in the laminar regime. The heat transfer is enhanced in a particular range of the Dean number [60–1000], without significant increase in the pressure drop (Mokrani et al., 1998a,b).

This flow finds applications in the pharmaceutical industry or food industry to process highly viscous fluids or fluids with stress-sensitive long molecular chains. The purpose of this study is to investigate the capacity of chaotic advection to generate liquid/liquid dispersion.

An experimental study was undertaken in order to observe the effect of chaotic advection on the dispersion of water in a laminar oil flow, and also to obtain experimental data for validation of the results of a theoretical approach to the water–oil dispersion in this flow. The theoretical approach is based on the determination of drop equilibrium under the joint action of viscous stresses generated by chaotic advection flow and interface tension.

In a curved pipe, the centrifugal force induces a secondary flow in the form of counter-rotating cells called Dean roll-cells that are superimposed on the axial flow and play the role of internal agitators of the flow. Analytical solutions for Dean flow have been proposed by Jones et al. (1989) and Le Guer and Peerhossaini (1991).

In the present work, the theoretical determination of the equilibrium drop size is based on Taylor's analysis (Taylor, 1953) as extended by Grace (1982). From this it is possible to compute the Eulerian distribution of the strain rates in the pipe cross-section, and to propose a model for the maximum shear and elongation rates introduced in Grace's work (1982) to calculate the theoretical maximum diameters with no fitting constant. The additional forces introduced by Dean flow above a certain Dean number generate stresses due to stretching and folding that are over and above the basic strain rates in the straight pipe, and these stresses enhance the breakup of water drops injected into the main oil flow.

* Corresponding author. Tel.: +33 2 40 68 31 24; fax: +33 2 40 68 31 41.
E-mail address: hassan.peerhossaini@univ-nantes.fr (H. Peerhossaini).

0301-9322/$ - see front matter © 2009 Elsevier Ltd. All rights reserved.
doi:10.1016/j.ijmultiphaseflow.2009.02.019

From this point of view, there is no theoretical difference between the helically coiled and twisted-pipe chaotic advection configurations. The drop diameters predicted by the theoretical approach are then compared with the experimental values for the three configurations (straight, helically coiled, and twisted-pipe flows).

A Lagrangian analysis of the flow was undertaken to explain the finer drop size observed experimentally in the chaotic advection flow. A comparison of the trajectories and of the Poincaré section of the fluid particles after 25 bends, for helically coiled and chaotic advection flows, qualitatively confirms that the latter configuration provides better macro-mixing. This feature is clear in the residence time distribution (RTD) for the two configurations and helps to explain the better dispersive performance of the chaotic advection flow. An illustration for $De = 100$ shows the improved homogenizing properties of the chaotic advection configuration.

This paper is organized as follows. In Section 2 the experimental setup and experimental results for the water–oil dispersion are presented. Section 3 is devoted to the theoretical prediction of droplet diameters by an Eulerian approach. The mechanical history of droplets in the flow determined by Lagrangian approach is given in Section 4, as is a presentation of the resident time distribution of fluid particles. Conclusions are drawn in Section 5.

2. Experimental setup and methods

2.1. Experimental setup

As shown in Fig. 1, the test section is composed of a succession of 90° bends with a given curvature radius. It can be arranged in both the helically coiled pipe and the twisted-pipe configurations where each bend is rotated in the orthogonal plane with respect to the preceding one, as seen in Fig. 2. Both geometries have 25 bends of 8 mm inside diameter D, the same unfolded length ($L = 2$ m) and the same bend curvature radius ($R = 44$ mm). The straight pipe has also an inside diameter of $D = 8$ mm and unfolded length $L = 2$ m. The dimensions of the test section are given in Table 1.

A schematic diagram of the hydraulic loop used here is shown in Fig. 3a. It has four main elements:

- oil admission circuit;
- water injection system;
- test section;
- flow visualization device at the test section exit.

The tank contains 100 L of a vegetable oil, allowing experimentation for 1 h at a Reynolds number of $Re = 50$ and 5 min at $Re = 600$. The flow rates are measured by rotameters with 5% accuracy (Sart Von Rohr SAS™ for water and Krohne Dusburg™ for oil).

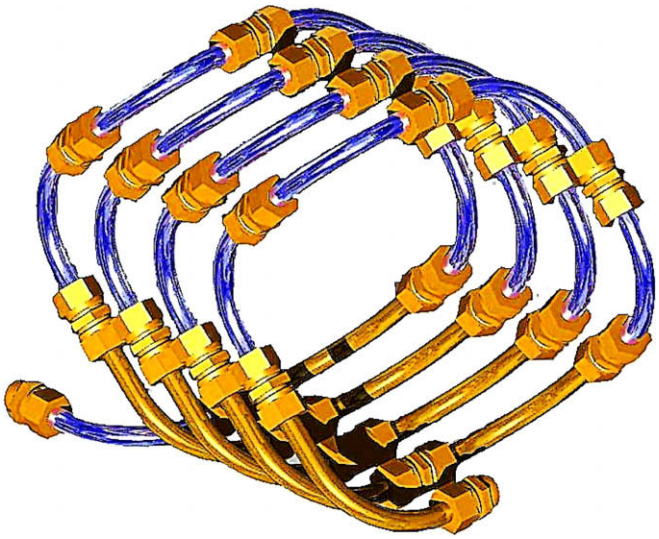

Fig. 2. Twisted pipe test section.

Table 1
Test section dimensions.

Diameter of circular duct	8 mm
Bend curvature radius	44 mm
Curvature angle in bend plane	$\frac{\pi}{2}$ rad
Number of bends	25
Total curved length	1.8 m
Straight length between bends	0.2 m
Total length	2 m

The oil is pumped by a centrifugal pump, while the water is supplied by a constant-level feed tank connected to the water supply network. The flow rate is monitored by a back-pressure valve. Water is injected at the twisted pipe inlet by an injection needle of inside diameter 2 mm, designed so that the velocity ratio (injection/main flow) does not exceed 1.5 for the most extreme conditions (water volume fraction of 10%). The current volume fractions are much lower, so that perturbations at the injection might not induce an additional breakup of the water droplets.

2.2. Drop size measurement

The flow visualization system (Fig. 3b) is a rectangular Plexiglas™ window positioned on top of a parallelepipedic box,

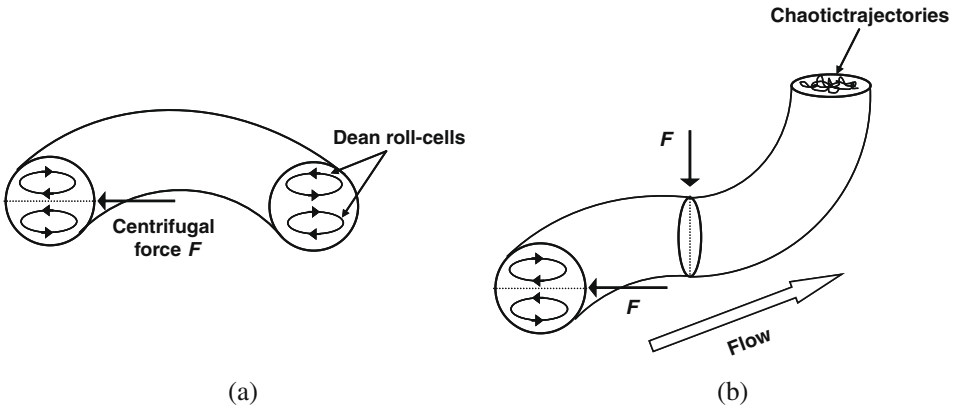

Fig. 1. Generation of spatially chaotic particle paths in laminar, steady, and three-dimensional flow: (a) regular Dean flow; and (b) twisted pipe Dean flow.

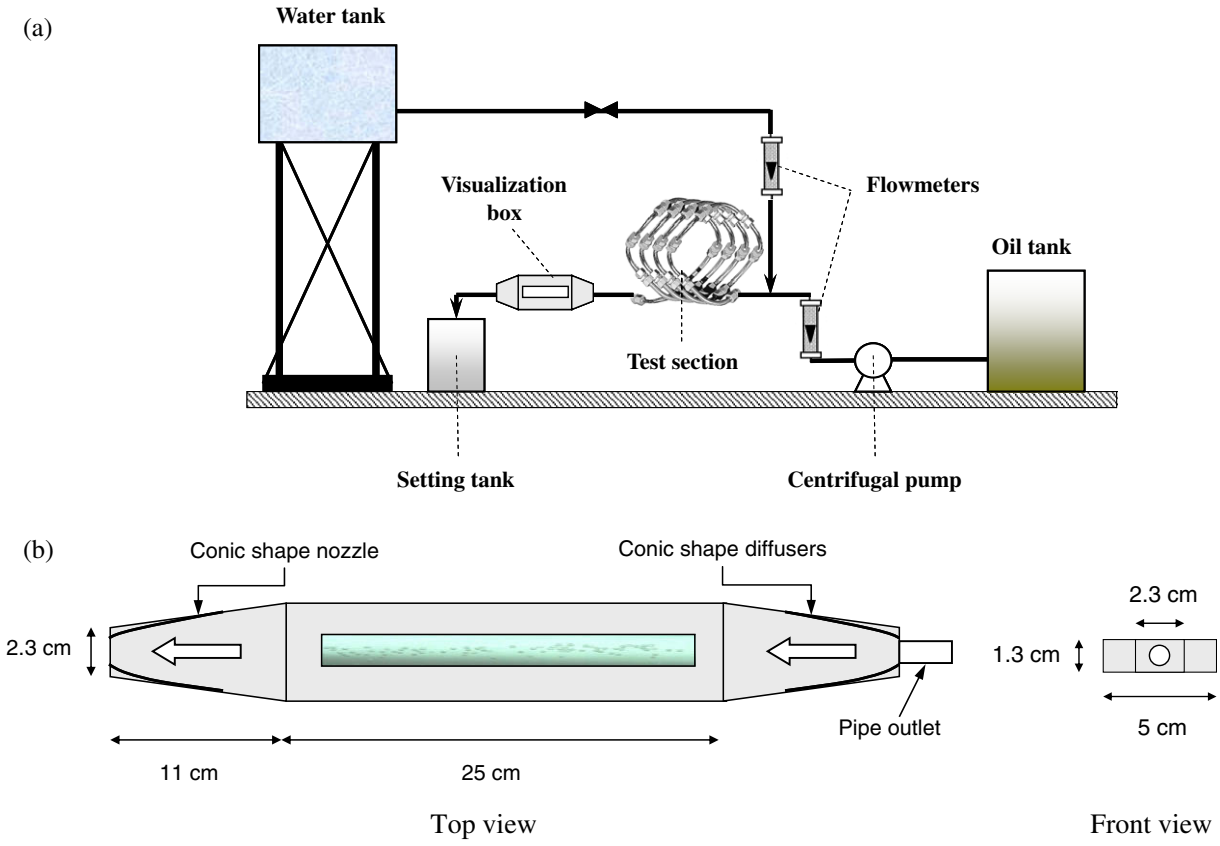

Fig. 3. (a) Schematic diagram of experimental setup. (b) Flow visualization system.

with conic/rectangular connections at each end. At the entrance, directly at the exit of the test section, the diffuser, is designed to minimize flow disturbances by maintaining (as much as possible) the shear stresses at the same level as in the test section, and, with a 7° angle, to avoid recirculations at low flow rates and thus to prevent drop coalescence at the pipe exit. Moreover, the box depth is small enough (depth is 13 mm, equals to 1.625 D) to prevent drops overlapping. In fact overlapping did not occur for the range of flow rates in this experiment, but may occur for higher flow rates.

Pictures of the emulsion are taken with a high-frequency digital Canon™ camera placed vertically above the visualization window with its optical axis perpendicular to the window's plane. The emulsion flow in the visualization box is lit from below by an intense diffuse white light. For given operating conditions, a sequence of independent images is selected and recorded; this sequence, an example of which is shown in Fig. 4, constitutes our statistical sample of the drops. Drop diameters are measured from the recorded images using IMAQ Vision Builder 6 software. At the end of the analysis, a table of diameters of at least 400 drops for each run is obtained. The experimental size distributions are fitted with a log-normal law. By taking 99% of the cumulative volume curve, a representative value for the maximum diameter can be determined. The standard deviation factor is also of interest for the quality of the emulsification process in further applications. If k is the log-standard deviation, the linear deviation β can be deduced from

$$\beta = \sinh(k) \tag{2}$$

Measurements were carried out for the three configurations: straight pipes, helically coiled pipes, and twisted pipes. By the log-normal law, the maximum drop diameter is found by reading 99% from the frequency of the cumulative diameter values on the fitted log-normal curve, as shown in Fig. 5 for a straight tube.

2.3. Working fluids

The continuous phase is commercial food-grade vegetable oil, and tap water is injected as the dispersed phase. The kinematic viscosity of the oil was measured using a Mettler™ RM180 rheometer. To measure the surface tension of the working fluid we used the Wilhelmy method: a metallic blade suspended from a balance by a stem is plunged into the liquid; the balance measures the vertical

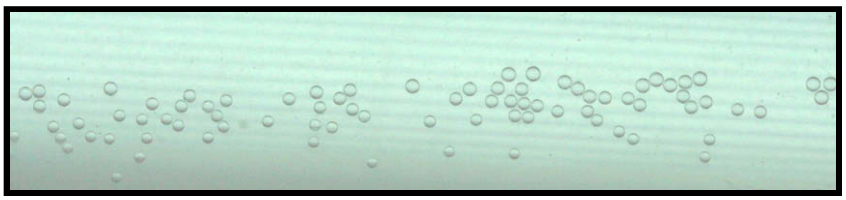

Fig. 4. Image of droplets taken by fast digital camera (chaotic advection configuration – oil flow rate $Q = 50\,\mathrm{l\,h^{-1}}$).

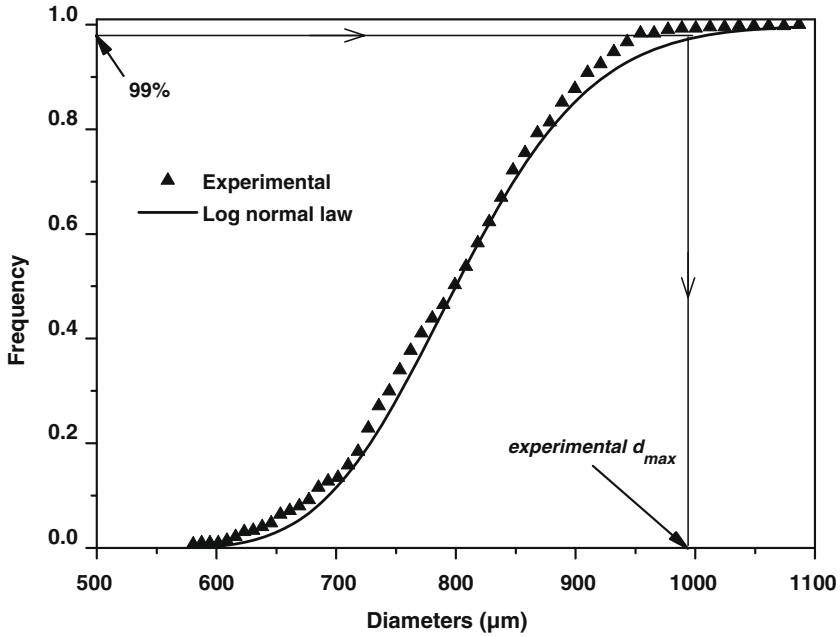

Fig. 5. Experimental droplet diameter distribution fitted by log-normal curve (straight pipe with oil flow rate $Q = 80\,\mathrm{l\,h^{-1}}$).

force F exerted on the stem by withdrawing the blade from the liquid. The surface tension σ is calculated by:

$$F = \sigma\zeta\cos\theta \tag{3}$$

where ζ is the wet perimeter. The platinum blade is previously passed through a flame to obtain perfect adhesion to the liquid surface. The ideal contact angle is $\theta = 0°$, for which the term $\cos\theta$ in Eq. (2) tends to 1. Therefore the value of the surface tension σ can be deduced from the geometric characteristics of the blade.

As the oil viscosity μ_c is very sensitive to temperature and has significant consequences on the dispersion through the viscous stress, the oil temperature T was controlled by a Chromel/Alumel (type K) thermocouple in the oil admission circuit. For modelling purposes, oil viscosity was measured with an AR1000 TA Instr™ rheometer and fitted by Arrhenius' law:

$$\mu_c = \mu_{c_0}\exp\left(\frac{E}{RT} - \frac{E}{RT_0}\right) \tag{4}$$

where $E = 29$ kJ, $R = 8.314\,\mathrm{J\,K^{-1}\,mol^{-1}}$ and μ_{c_0} is the oil viscosity for a given temperature T_0. The physical properties of the two fluids are given in Table 2.

2.4. Reproducibility

Runs were repeated three times on different days to check the effect of a new operator and a new trial on the measured characteristics of the final emulsion in the test section. Nominal operating conditions at Dean number $De = 70$; the resulting size distributions of the three runs were compared, leading to a maximum error of ±6% in the maximum drop diameter.

Table 2
Characteristics of working fluids used in experiments.

Interfacial tension	$0.0192\ \mathrm{N\,m^{-1}}$
Oil density	$910\ \mathrm{kg\,m^{-3}}$
Water density	$1000\ \mathrm{kg\,m^{-3}}$
Water dynamic viscosity	0.001 Pa s
Oil dynamic viscosity at 25 °C	0.052 Pa s
Viscosity ratio	0.0192

2.5. Experimental results for drop diameters

Drop size distributions were measured for the three configurations: straight, helically coiled and twisted pipes. A summary of the results is given in Table 3.

The maximum drop diameters are plotted versus the oil flow rate in Fig. 6. As expected, the drop diameters decrease with increasing flow rate, since the viscous stresses increase with yield velocity and velocity gradients. The water (dispersed phase) flow rate is not taken into account as an operating parameter unless it increases the global (two-phase) flow rate. This approximation is reasonable as long as we work with the lowest injection rate (about 5% volume fraction) to minimize flow disturbance at the injection point and to prevent drop coalescence: at this level, the dispersed phase volume fraction does not influence the drop breakup. The drop diameters obtained in the chaotic flow are smaller than those in the helically coiled flow, the latter being smaller than that in the straight tube.

For an oil flow rate of about $100\,\mathrm{l\,h^{-1}}$, a transition can be observed on the drops diameters in the twisted pipe chaotic flow. In fact, at this stage, which corresponds to a Dean number of about 60, the chaotic advection becomes significant. These results confirm the idea that the chaotic advection flow improves the liquid/liquid dispersion.

For the same runs, the standard deviation of the drop size distribution, shown in Fig. 7, is about 20% less for the twisted pipe than for the helically coiled pipe. This trend appears more clearly

Table 3
Measured maximum droplet diameters.

Flow rate ($\mathrm{l\,h^{-1}}$)	Straight pipe (mm)	Helically coiled pipe (mm)	Chaotic twisted pipe (mm)
40	1.58	1.39	1.28
50	1.56	1.24	1.11
60	1.20	1.12	1.01
70	1.19	1.08	0.94
80	0.98	0.92	0.84
90	0.96	0.89	0.79
100	0.84	0.79	0.57

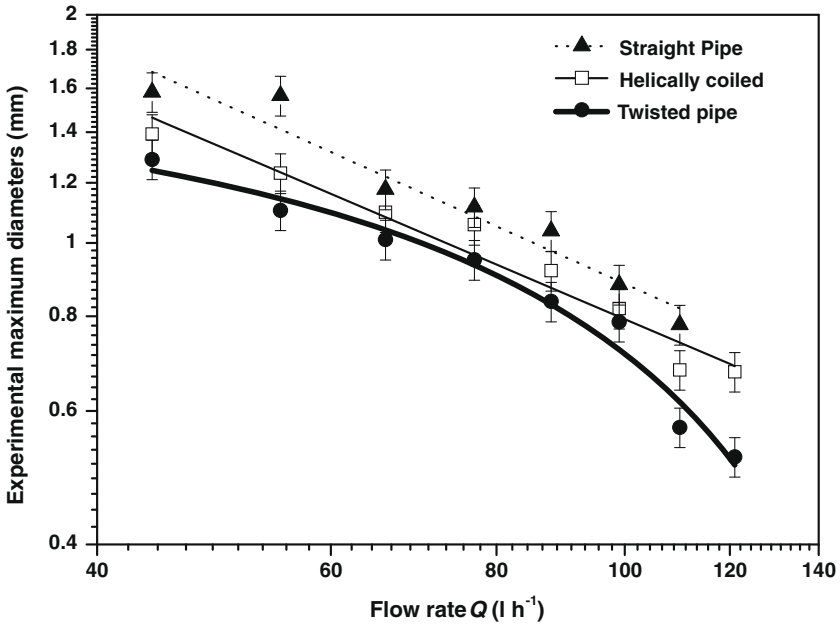

Fig. 6. Experimental d_{max} versus oil flow rate.

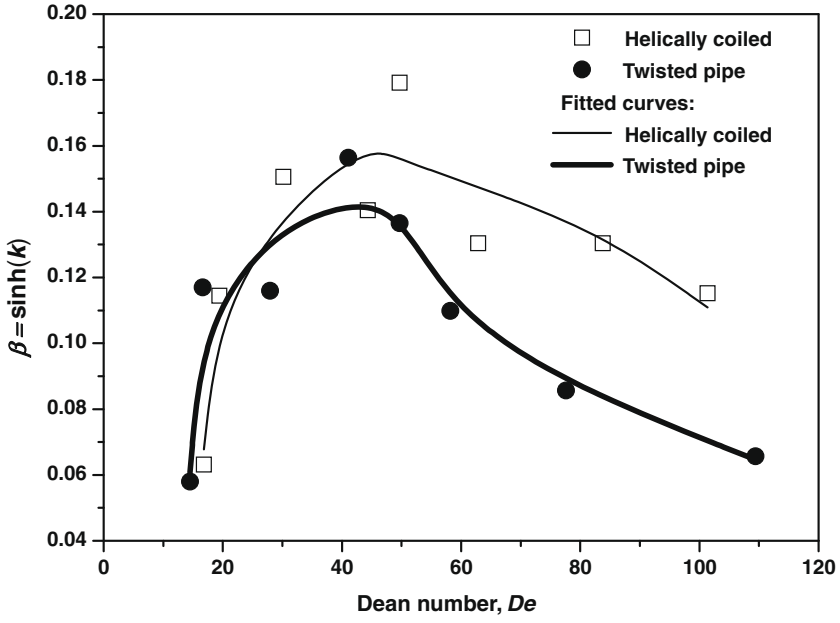

Fig. 7. Droplet diameter dispersion factor for helically coiled and chaotic twisted pipe – curves fitted using Savitzky–Golay method.

for Dean numbers higher than 50, where the chaotic behaviour begins to induce strains of the same magnitude as the shear flow. The standard deviation seems minimal at low Dean numbers where the mixing process is globally homogeneous over the whole test section but has the lowest mixing efficiency. Increasing the Dean number increases the standard deviation; i.e. the non-homogeneity of the observed emulsion is increased because of the poor radial distribution of the fluid in the mixer cross-section until an effective Dean number is achieved at which the homogeneity and mixing efficiency are intensified.

The Sauter mean diameter d_{32} is a statistical parameter that can be used to characterize the drop size distribution in the flow. This diameter, given in Eq. (5), represents the mean surface diameter:

$$d_{32} = \frac{\int \ell^3 f(\ell)\, d\ell}{\int \ell^2 f(\ell)\, d\ell} \tag{5}$$

where $f(\ell)$ is the distribution function representing the proportion of drops having a given diameter ℓ in the observed emulsion.

The proportionality between the Sauter mean diameter d_{32}, and the maximum drop diameter d_{max} is represented in Fig. 8. The experimental results show that the d_{32} and d_{max} diameters are linearly correlated in the limit of validity, here $10 < De < 110$. When the slope of the fitted line is equal to one it implies that the Sauter mean diameter is equal to the maximum drop diameter, and therefore that the drop fragmentation is uniformly distributed over the whole observed emulsion. The more this coefficient is close to 1,

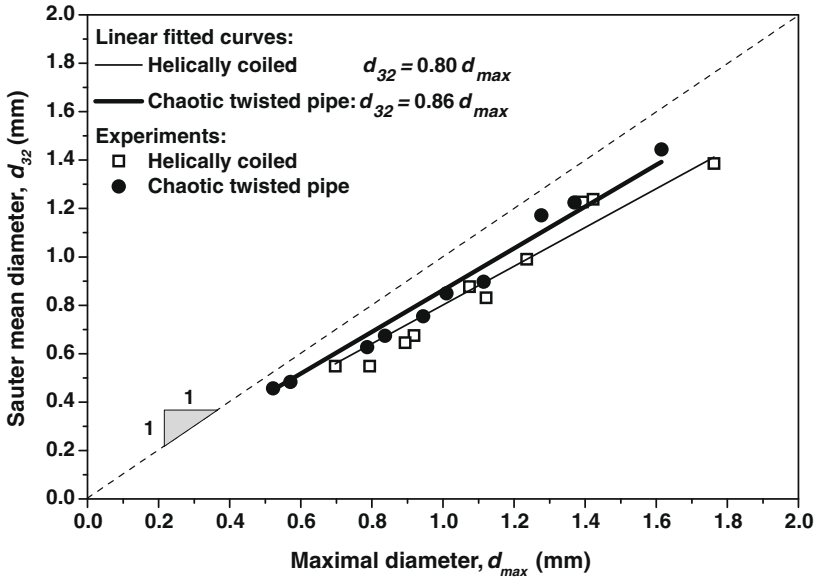

Fig. 8. Sauter mean diameter versus maximal diameter of droplets in helical coiled and chaotic advection twisted pipes.

the sharper is the distribution. It was found by Zhou and Kresta (1998) that the slope value for agitated tanks and bent tubes equipped with a static mixer is between 0.38 and 0.7; these values are much smaller than that in the present work, meaning a much less homogeneous droplet size distribution.

To investigate the efficiency of helically coiled and chaotic twisted pipe flows, the energy cost is compared in Fig. 9 with that of existing inline mixers reported by previous investigators (Haas, 1987; Streiff et al., 1997; Lemenand et al., 2003, 2005).

The interfacial contact area A is given by the Sauter diameter:

$$A = \frac{6\Phi}{d_{32}} \tag{6}$$

where Φ is the mass fraction of the dispersed phase.

The energy consumption E is calculated from the pressure drop ΔP:

$$E = \frac{\Delta P}{\rho} \tag{7}$$

The pressure drop ΔP is obtained from the theoretical correlation of Ito (1969) for laminar flow in curved pipes.

From Fig. 9, the helically coiled and chaotic twisted pipe flows are located in the small-energy consumption zone (between 1 and 12 J kg^{-1}) with a good interfacial area (between 300 and 1100 m^2 m^{-3}). The Sulzer mixer seems to have the highest interfacial area but in the range of high energy consumption. The HEV has the same behavior as the geometries studied in the present work, which are both better than Kenics static mixer.

The very low energy consumption and the relatively good interfacial contact show that helically coiled and chaotic twisted pipe flows can have good impacts in the industrial applications, especially when mixing fluids that cannot tolerate high shear rates.

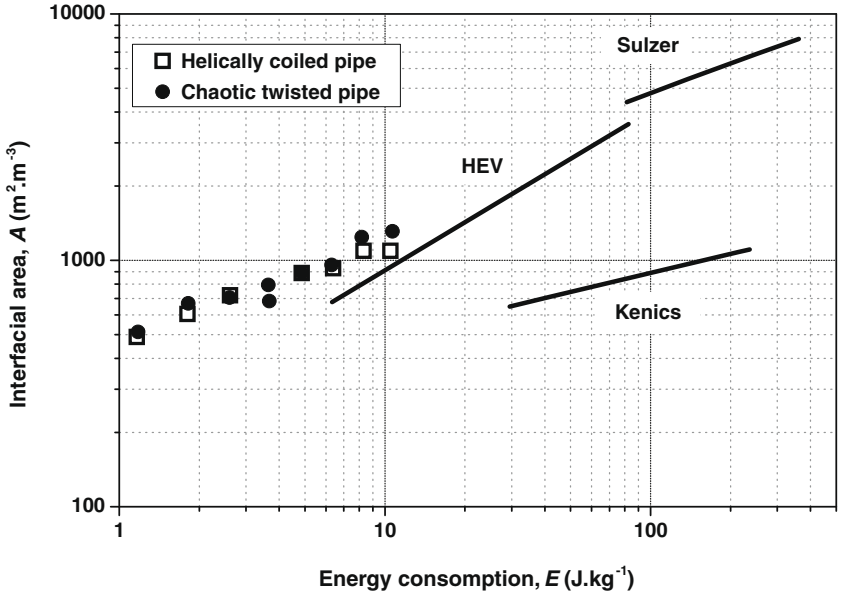

Fig. 9. Comparison of the energy consumption of the helically coiled and chaotic twisted pipes with classical static mixers (data from Thakur et al., 2003).

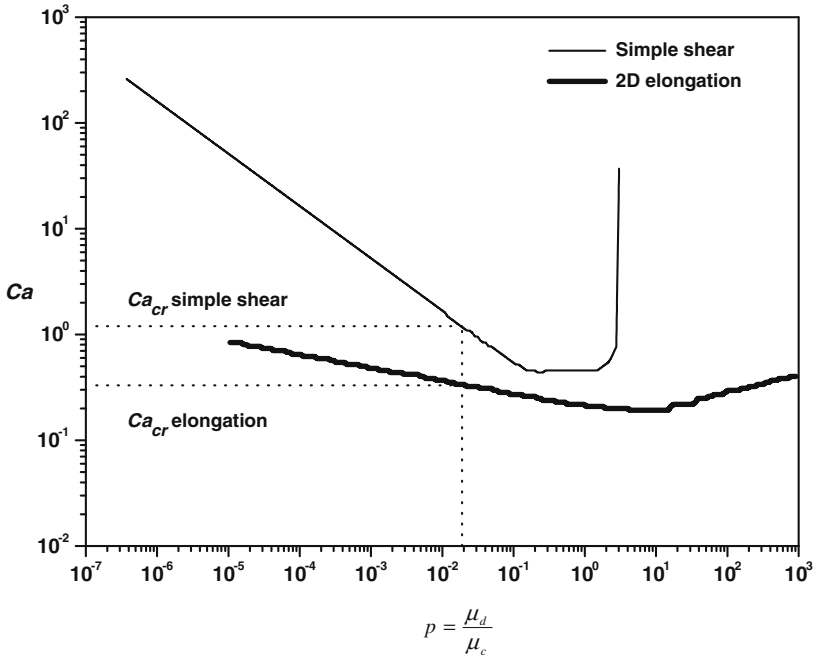

Fig. 10. Critical capillary number for shear and elongation rates; curves adapted from Grace (1982).

3. Theoretical prediction of drop diameters

3.1. Breakup theory for laminar flows

The Taylor theory for drop breakup is based on a balance among the following forces acting on a single drop of an immiscible fluid in a continuous fluid flow:

- The external viscous flow forces that tend to deform the drop; for example, in a shear flow the viscous flow force can be written as:

$$\tau = \mu_c \dot{\gamma} \tag{8}$$

  where $\dot{\gamma}$ is the shear rate.
- The interfacial or capillary forces that tend to preserve the spherical shape of a drop of diameter d_{drop}; the pressure difference at the interface balances the interfacial tension σ as expressed by the Laplace formula

$$P_{\text{int}} - P_{\text{ext}} = \frac{4\sigma}{d_{\text{drop}}} \tag{9}$$

  (P_{int} and P_{ext}) are the interior and the exterior pressures, respectively.
- The internal viscous forces that resist deformation.

In order to characterize the relative effect of the different forces, a dimensionless parameter Ca (the capillary number) is defined:

$$Ca = \frac{\text{Viscous forces}}{\text{Capillary forces}} = \frac{d_{\text{drop}}\tau}{2\sigma} \tag{10}$$

Grace (1982) considered that drop breakup occurs when the capillary number exceeds a critical value that depends upon the viscosity ratio (the dispersed-phase viscosity by the continuous-phase viscosity) as the manifestation of the drop's internal viscous resistance.

The dimensional values of the maximum diameter that can withstand an existing stress τ can hence be expressed by the equation

$$d_{\max} = \frac{2\sigma}{\tau} Ca_{\text{cr}} \tag{11}$$

The critical capillary numbers are given by the Grace experimental curves (Fig. 10) for simple shear flows ($Ca_{\text{cr,shear}}$) and elongational flows ($Ca_{\text{cr,elongation}}$). The effective capillary number in laminar dispersion phenomena depends on the critical capillary number, Ca_{cr}, of both simple shear and elongation, and on the ratio of these deformation rates $\Gamma = \dot{\varepsilon}_{\max}/\dot{\gamma}_{\max}$.

By making simple linear interpolation we can find Ca_{cr} from the following expression:

$$Ca_{\text{cr}} = (1-\Gamma) Ca_{\text{cr,shear}} + \Gamma Ca_{\text{cr,elongation}} \tag{12}$$

Knowing the viscous stresses, we obtain the Γ value, and by substituting Eqs. (8) and (12) in Eq. (11), we can predict the maximum equilibrium diameter of the drop size distribution.

3.2. Determination of the strain rates in Dean flow

The analytical expressions for the velocity field in Dean flow in a curved channel were obtained from Dean's asymptotic solution (Dean, 1928). In the present work, the analytical solution was calculated from the stream function given by Jones et al. (1989) expressed in a local frame of reference, as shown in Fig. 11. All computations were carried out with MATLAB™. Table 4 presents the dimensionless variables involved in the analysis.

As in all the previous work, the parabolic axial velocity profile is assumed

$$w = 2\frac{R}{a}(1-r^2) \tag{13}$$

The potential stream function in the cross-section is given by

$$\psi = \frac{R}{Wa^2}\frac{vDe}{72}(4-r^2)(1-r^2)^2 y \tag{14}$$

where $r^2 = x^2 + y^2$ is the radial coordinate in the tube cross-section, v the effective kinematic viscosity, and W the flow mean velocity.

In the local coordinate system (x, y, z), the secondary velocity u and v can be written as

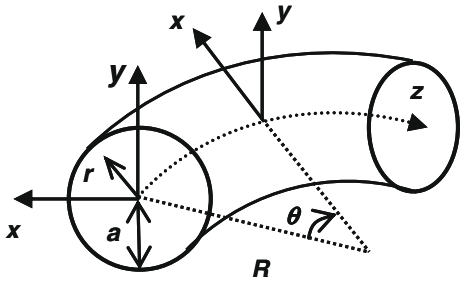

Fig. 11. Toroidal coordinates.

Table 4
Flow variables.

	Dimensionless variable	Dimensional variable
Radial distance	r	$r' = ar$
Time	t	$t' = \frac{R}{W}t$
Coordinate	x	$x' = ax$
Coordinate	y	$y' = ay$
Axial coordinate	z	$z' = az$
Velocity component	u	$u' = a\frac{W}{R}u$
Velocity component	v	$v' = a\frac{W}{R}v$
Axial velocity	w	$w' = a\frac{W}{R}w$
Shear rate	$\dot{\gamma}$	$\dot{\gamma}' = \frac{W}{R}\dot{\gamma}$
Elongation rate	$\dot{\varepsilon}$	$\dot{\varepsilon}' = \frac{W}{R}\dot{\varepsilon}$
Stream function	$\psi = \frac{R}{Wa^2}\frac{vDe}{72}(4-r^2)(1-r^2)^2 y$	$\psi' = \frac{Wa^2}{R}\psi$
Reynolds number	$Re = 2\frac{Wa}{v}$	
Dean number	$De = \frac{a}{4R}Re^2$	

$$u = \frac{\partial\psi}{\partial y} \qquad v = -\frac{\partial\psi}{\partial x} \tag{15}$$

which leads to the following two equations:

$$\begin{aligned} u &= \alpha(1-r^2)[6y^2(3-r^2) - (4-r^2)(1-r^2)] \\ v &= -6\alpha xy(1-r^2)(3-r^2) \end{aligned} \tag{16}$$

where $\alpha = \frac{Re}{144}$.

For the fully developed flow, the velocity field in the pipe cross-section appears to be independent of z. The effect of the radius of curvature is not explicit in this system because of the dimensionless scaling of the coordinates.

The generalized shear rate $\dot{\gamma}$ and elongation rate $\dot{\varepsilon}$ given by Eq. (17), and calculated from the analytical derivatives of the velocity components, are given in Germain (1962) and also in Bird (2007), and are defined, respectively, as the second invariant of the deformation rate tensor and the extension along the axis carried by the first eigenvector of the deformation rate tensor. These expressions are also used by Khakhar and Ottino (1986).

$$\begin{cases} \dot{\gamma} = \left(2\left(\frac{\partial u}{\partial x}\right)^2 + 2\left(\frac{\partial v}{\partial y}\right)^2 + 2\left(\frac{\partial w}{\partial z}\right)^2 + \left(\frac{\partial u}{\partial y} + \frac{\partial v}{\partial x}\right)^2 \right. \\ \qquad \left. + \left(\frac{\partial u}{\partial z} + \frac{\partial w}{\partial x}\right)^2 + \left(\frac{\partial v}{\partial z} + \frac{\partial w}{\partial y}\right)^2\right)^{1/2} \\ \dot{\varepsilon} = \frac{u^2\left(\frac{\partial u}{\partial x}\right) + v^2\left(\frac{\partial v}{\partial y}\right) + w^2\left(\frac{\partial w}{\partial z}\right) + uv\left(\frac{\partial u}{\partial y} + \frac{\partial v}{\partial x}\right) + uw\left(\frac{\partial u}{\partial z} + \frac{\partial w}{\partial x}\right) + vw\left(\frac{\partial v}{\partial z} + \frac{\partial w}{\partial y}\right)}{u^2 + v^2 + w^2} \end{cases} \tag{17}$$

In a flow, it is the maximal value of the shear and elongation rates, $\dot{\gamma}_{\max\ \text{helic}}$ and $\dot{\varepsilon}_{\max\ \text{helic}}$, that determine the droplets' maximum diameter. These values are obtained from Eq. (17) and are expressed as:

$$\begin{cases} \dot{\gamma}_{\max\ \text{helic}} = 4\frac{R}{a}\left[1 + \frac{1}{150}\frac{a}{R}De\right]^{0.5} \\ \dot{\varepsilon}_{\max\ \text{helic}} = 1.1\frac{R}{a}\left[1 + 2\times 10^{-7}\frac{a}{R}De^3\right]^{0.7} \end{cases} \tag{18}$$

The classical dimensionless maximal shear rate for the straight pipe is given by

$$\dot{\gamma}_{\max\ \text{straight tube}} = 4\frac{R}{a} \tag{19}$$

For the range of Dean numbers studied here, the maximum shear and elongation rates in the flow cross-section fitted with trend curves (Eqs. (18) and (19)) are presented in Fig. 12 for use in the dispersion model. It can be noted that, following the analytical solution, the helical-pipe flow shear rate begins to deviate from that of the straight pipe flow at an estimated Dean number around $De = 55$. On the other hand, for a Dean number of about 600, the elongation rate begins to dominate the shear rate and governs the dispersion process. This would lead to a decrease of 1/3 in the diameter and would enhance the eventual benefits of the chaotic advection flow. This range of Dean number, however, cannot be achieved in the present experimental setup and will not be discussed further.

The theoretical maximum diameters of the drops can be calculated by using Eq. (11) coupled with the above maximum shear rates (Eqs. (18) and (19)). Theoretical and experimental maximum diameters are compared in Fig. 13. The theoretical curve is unique for the twisted-pipe flow (chaotic advection) and the helically coiled pipe flow, since the Eulerian velocity fields are the same in both cases.

The experimental maximum diameters of the drops are also shown in Fig. 13. At least a part of the discrepancy between experimental and theoretical results can be explained by the numerous hypotheses of the theoretical models, both the Taylor–Grace model (based on an assumed dynamic equilibrium situation) and the Dean–Jones equations (which give an approximate solution for the velocity field). Nevertheless, the maximum global difference with experimental results does not exceed 10%, showing that the present theoretical approach captures the basic physics underlying the problem.

It can be noticed in Fig. 13 that the maximum drop diameters measured in the chaotic flow are smaller than in the helically coiled pipe flow, suggesting that, in addition to the deformation rates responsible for drop breakup in the helically coiled pipe flow, there exists another mechanism that leads to better drop fragmentation in the chaotic advection flow. It is shown in the next section through a Lagrangian analysis that this mechanism is, in fact, the way in which droplets are randomly passed to zones of higher shear and strain rates in the chaotic advection flow compared to the helically coiled flow.

4. Lagrangian analysis of the flow

4.1. Mechanical history

This Lagrangian study is based on following a fluid particle trajectory from its initial location at the inlet up to the outlet, as well as on tracking the shear and elongations to which it is submitted, i.e. its "mechanical history". The Lagrangian equations for the passive advection of a fluid particle in a three-dimensional space are given by the following dynamical system:

$$\begin{cases} \dot{x} = u(x,y,z,t) \\ \dot{y} = v(x,y,z,t) \\ \dot{z} = w(x,y,z,t) \end{cases} \tag{20}$$

The equations are the same for helically coiled and twisted pipe flows. For the helically coiled pipe, there is no change of the frame reference axes while passing from one elbow to another. For the twisted pipe flow, the frame reference axes are rotated of ±90° as follows: at the end of each elbow of even number, a rotation of

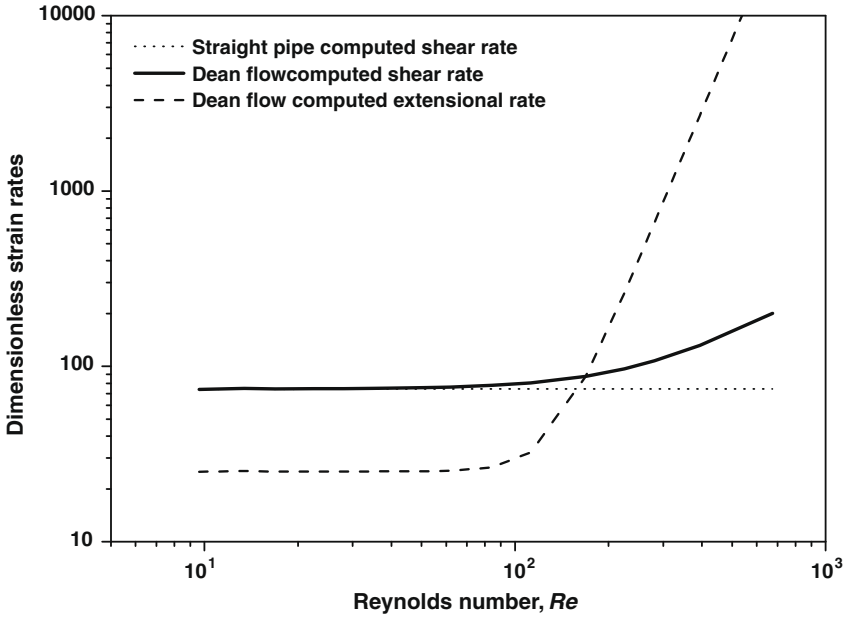

Fig. 12. Computed strain rates in straight pipe and helically coiled pipe – maximum values in pipe cross-section.

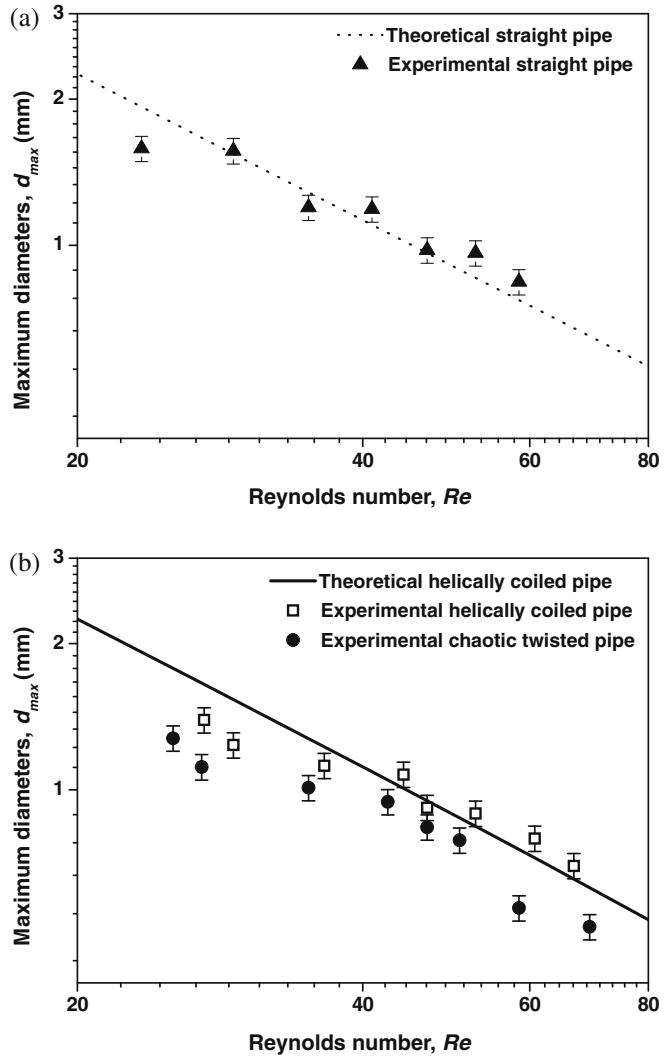

Fig. 13. Droplet diameters – experiments compared with theoretical values: (a) straight pipe, and (b) helically coiled and chaotic twisted pipes.

90° is applied to the reference axes (i.e. we replace x by y, and y by $-x$ in the velocity equations), otherwise, at the end of each elbow of odd number, a rotation of −90° is applied.

Integration along the trajectory is carried out in the numerical procedure by a fourth-order Runge–Kutta scheme. The passage of a particle from the outlet of one bend to the inlet of the next must be calculated very accurately; the convergence is realized by a Newton–Raphson iterative process.

The sensitivity of the trajectory to the time step dt was computed by studying the time step at which the solution converges to a constant value for different Dean numbers and the final position of the particle becomes independent of the maximal dt value given in

$$dt = \frac{\left(\frac{\pi}{2}\frac{R}{a}\right)}{W} \cdot 10^{-4} \tag{21}$$

Results for Dean number 150 are illustrated in Fig. 14, where the trajectories of a passive fluid particle in the helically coiled pipe flow are compared with those of a twisted-pipe flow along 25 bends and for two initial positions. In the chaotic flow, the particle sweeps all the cross-section of the pipe, while in helically coiled flow the particles remain on the same trajectory, depending on their initial positions. It can even be noted that in the helically coiled flow, for injection location $x_0 = 0$, $y_0 = 0.43$, the particle leaves the last bend at exactly the same cross-sectional position at which it entered the pipe; this point is the centre of the Dean roll-cell at which $u = v = 0$ and therefore there is no radial velocity.

Fig. 15 shows the Poincaré sections for the two configurations, helically coiled and chaotic, and for an initial position of a disk of diameter equal to 5% of the pipe cross-sectional diameter, made up of 5000 neighbouring points. It is observed again that in the helically coiled configuration, the particles remain in the Dean roll-cell, while in the chaotic advection case the particles spread over the whole tube cross-section. This has a direct consequence for the mechanical history of the fluid particle. In fact, along its chaotic trajectories the particle visits the zones of maximum shear and elongational rates. Figs. 16 and 17 show the particle's mechanical history, that is, the dimensionless shear and elongation rates that a fluid particle undergoes at each moment along 25 bends,

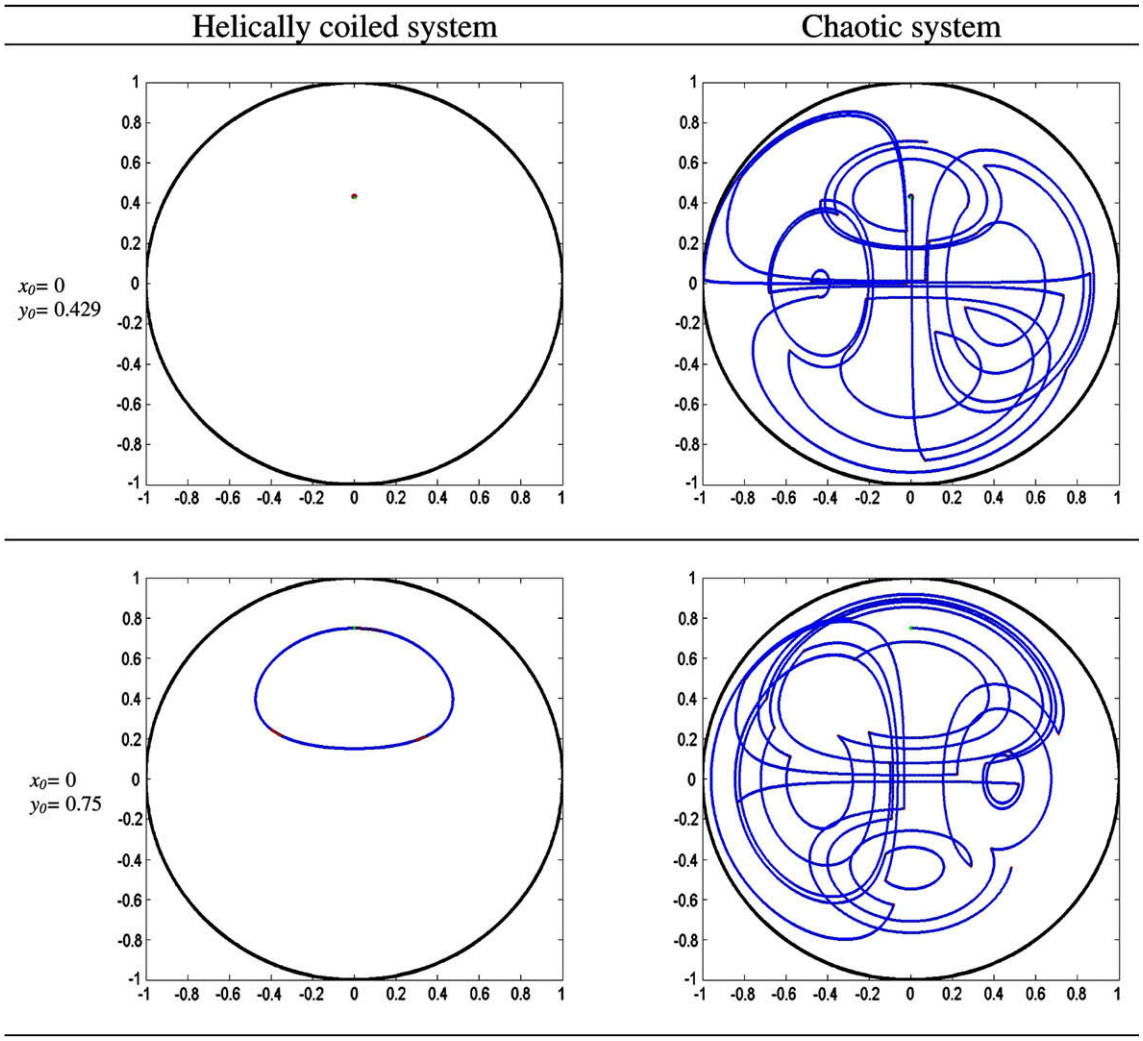

Fig. 14. Trajectories of passive tracer ($De = 150$, $Re = 81$, $Nc = 25$).

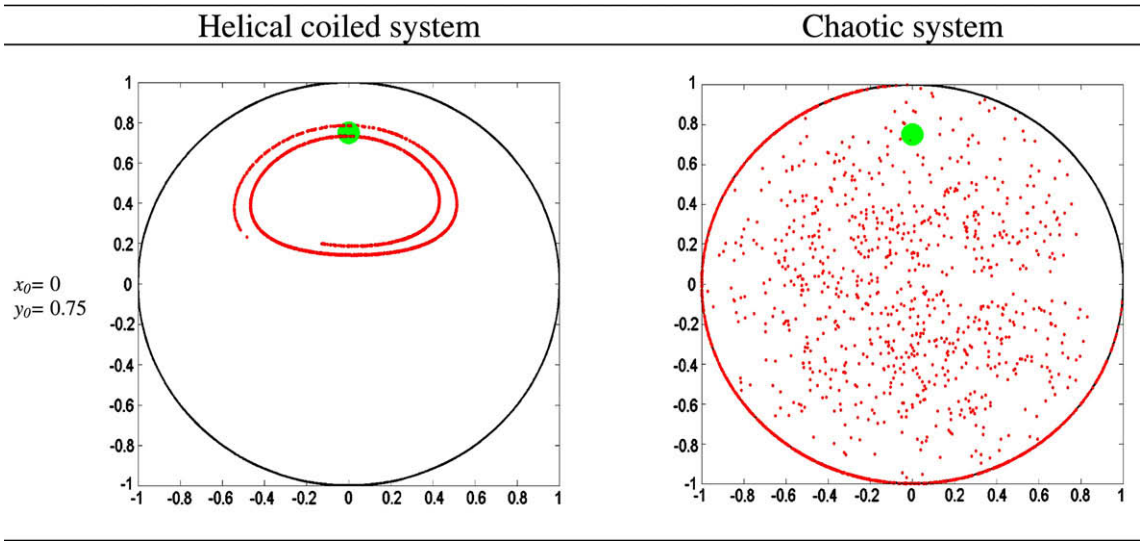

Fig. 15. Poincaré sections ($De = 150$, $Re = 81$, $Nc = 25$).

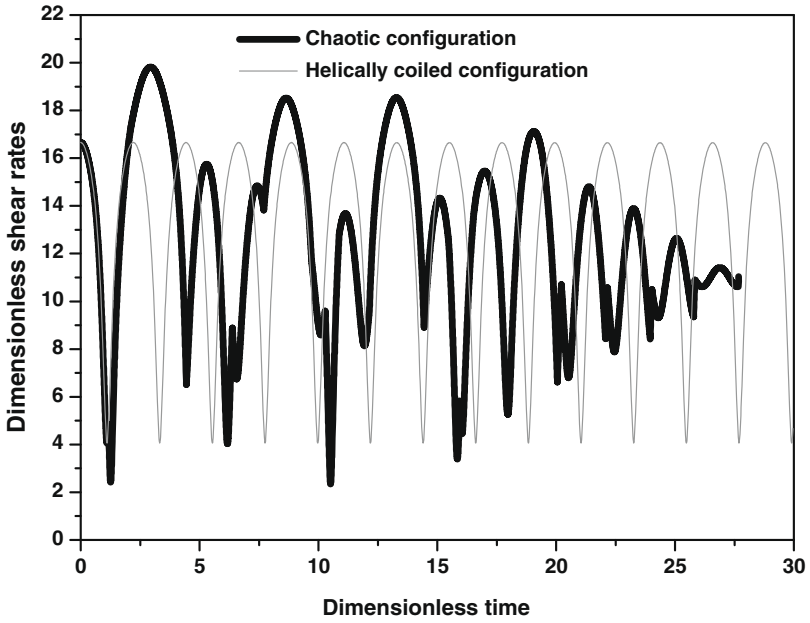

Fig. 16. Mechanical history of shear rates ($x_0 = 0$, $y_0 = 0.75$, $De = 100$).

for $De = 100$ and initial position $x_0 = 0$, $y_0 = 0.75$. In the helically coiled configuration, the particle has a periodic trajectory and remains caged between two limiting (maximum and minimum) values of the viscous stress. On the other hand, in a chaotic flow the particle randomly undergoes all levels of strain rates, especially the maximum values that are more efficient for drop breakup.

4.2. Residence time distribution (RTD)

The residence time distribution can be established by computing the trajectories for a sufficiently large number of particles (about 6000), which are uniformly distributed in the inlet plane section. Fig. 18 presents the RTD as a function of dimensionless residence time defined in Table 4 for helically coiled pipe flow and twisted-pipe chaotic advection flow. In this figure are also superposed the RTD for a straight pipe flow and an axial dispersed plug flow as expressed in Eqs. (22) and (23), respectively:

$$f(t) = \frac{1}{2}\left(\frac{Pe_L}{\pi\Theta}\right)^{\frac{1}{2}} \exp\left(-\frac{Pe_L(1-\Theta)^2}{4\Theta}\right) \tag{22}$$

$$f(t) = \frac{1}{2t\Theta^2} H\left(t - \frac{tm}{2}\right) \tag{23}$$

where t is the residence time, $t_m = \frac{L}{W}$ the mean residence time and $\Theta = \frac{t}{t_m}$ the reduced time.

It can be seen from Fig. 17 that even for a small Dean number of 100, while the helically coiled pipe flow presents a RTD profile similar to that of straight pipe, the RTD profile of the chaotic advection

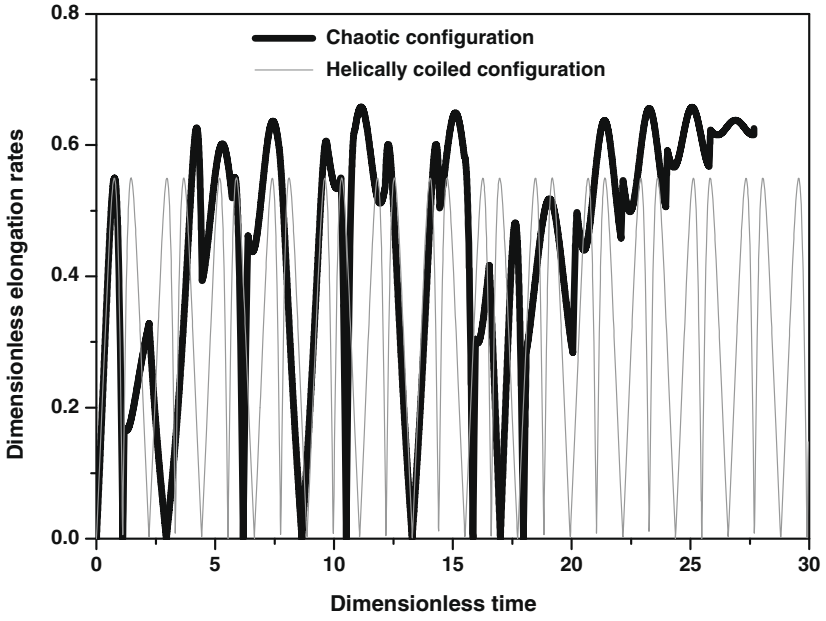

Fig. 17. Mechanical history of absolute elongation rates ($x_0 = 0$, $y_0 = 0.75$, $De = 100$).

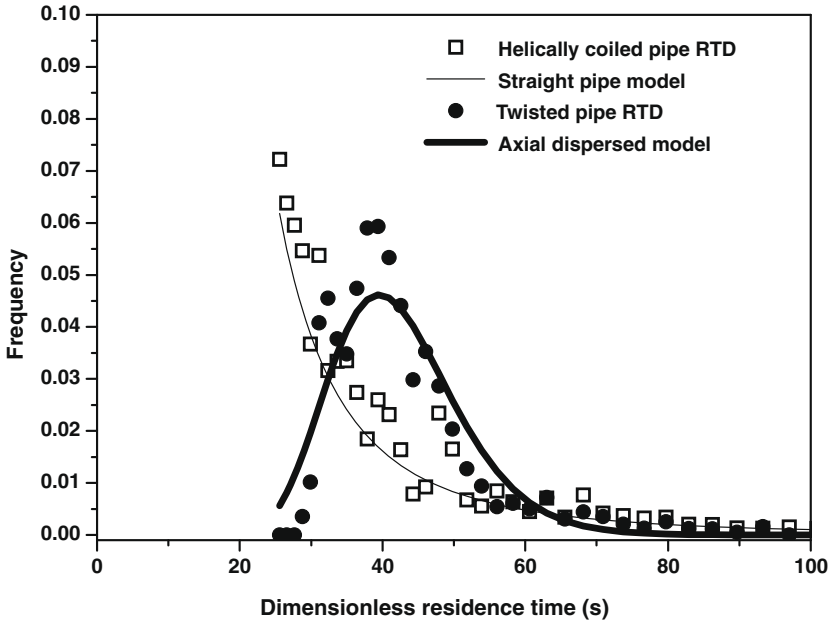

Fig. 18. Dimensionless residence time distribution: 25 bends for $De = 100$.

twisted pipe can be modeled by an axial dispersed plug flow. In this situation, the Péclet number based on the pipe length L, $Pe_L = \frac{WL}{D_{ax}}$, is about 43, where, D_{ax} is the axial diffusion coefficient.

In agreement with the trajectories presented in Fig. 13, the residence time dispersion is narrower in the chaotic advection configuration, accounting for the radial transfer enhancement. This result was also found by Castelain et al. (1997) in studying the RTD in chaotic twisted pipe and helically coiled pipe flows.

5. Conclusions

Careful experiments were carried out on liquid/liquid dispersion in oil/water flows to assess the effects of chaotic advection on droplet breakup, in terms of both the mean diameter and the size homogeneity. Both properties have strategic implications in many technological processes in the pharmaceutical and cosmetics industries, as well as in new biological renewable-energy processes. These experiments showed that the chaotic advection flow generated in the twisted pipe clearly increases the efficiency of contactors and mixers by providing smaller and more homogeneously dispersed droplets. The energy expenditure to obtain this dispersion remains similar to that of the rival technology, the helically coiled mixer.

To clarify the physical mechanism underlying this high dispersion efficiency of the chaotic advection flow compared to similar laminar flows, and also for the future design and optimization of multifunctional heat exchangers and reactors, a mechanistic modelling of this flow was undertaken. Both Eulerian and Lagrangian approaches were applied to three flow geometries in the laminar regime: straight, helically coiled and twisted pipes. While in most fluid dynamics problems the ultimate aim is to obtain the velocity field in the flow, in the chaotic advection problem the velocity field is the starting point. To this end, we used the analytical expression of the stream function in a curved pipe obtained by Dean (1927) as the building block of the model. Shear and elongation rates were then calculated and were used in conjunction with Taylor–Grace theory to study droplet breakup.

It was shown that the Eulerian approach cannot explain the higher dispersion efficiency of the chaotic advection flow. On the contrary, the Lagrangian approach allows calculation of the fluid particle trajectories and especially the "mechanical history" of a fluid particle. From this we showed that chaotic advection causes fluid particles to make random visits to zones of high shear and elongation rates and therefore contributes further to droplet breakup.

The model also allowed calculation of the RTD of fluid particles in helically coiled and twisted-pipe flows. The RTD analysis revealed that even for very small Dean number laminar flows, the chaotic advection flow shows a RTD distribution as narrow as an axially dispersed plug flow, while the helically coiled tube flow has a residence time distribution similar to a straight tube flow. Thus in liquid/liquid dispersion the chaotic advection flow has two principal advantages over its counterpart helically coiled pipe flow: first, generation of smaller droplets, second, a more homogenous droplet diameter distribution.

The mechanistic model developed in this work provides a solid basis for obtaining physical insight into dispersion phenomena by laminar flows and offers a powerful design and optimization tool to designers of future innovative devices. Future work will focus on gas/liquid dispersion by chaotic advection.

Acknowledgements

The authors gratefully acknowledge Dr. P. Carrière of LMFA (Laboratoire de Mécanique des Fluides et d'Acoustique) of École Centrale de Lyon (France), for fruitful and enlightening discussions.

References

Acharya, N., Sen, M., Chang, H.C., 1992. Heat transfer enhancement in coiled tubes by chaotic advection. Int. J. Heat Mass Transfer 35, 2475–2489.
Aref, H., 1984. Stirring by chaotic advection. J. Fluid Mech. 143, 1–21.
Bird, R.B., 2007. Transport Phenomena. Wiley, New York.
Castelain, C., Mokrani, A., Legentilhomme, P., Peerhossaini, H., 1997. Residence time distribution in twisted pipe flows: helically coiled system and chaotic system. Exp. Fluids 22, 359–368.
Dean, W.R., 1927. Note on the motion of fluid in curved pipe. Philos. Mag. 4, 208–227.
Dean, W.R., 1928. The streamline motion of fluid in curved pipe. Philos. Mag. 5, 673–695.
Germain, P., 1962. Mécanique des milieux continues. Ed. Masson.

Grace, H.P., 1982. Dispersion phenomena in high viscosity immiscible fluid systems and application of static mixers as dispersion devices in such systems. Chem. Eng. Commun. 14, 225–277.
Haas, P.A., 1987. Turbulent dispersion of aqueous drops in organic liquids. AIChE J. 33, 987–995.
Ito, H., 1969. Laminar flow in curved pipes. Z. Angew. Math. Mech. 11, 653–663.
Jones, S.W., Thomas, O.M., Aref, H., 1989. Chaotic advection by laminar flow in a twisted pipe. J. Fluid Mech. 209, 335–357.
Khakhar, D.V., Ottino, J.M., 1986. Deformation and breakup of slender drops in linear flows. J. Fluid Mech. 166, 265–285.
Le Guer, Y., Peerhossaini, H., 1991. Order breaking in Dean-flow. Phys. Fluids A 3, 1029–1032.
Le Guer, Y., Castelain, C., Peerhossaini, H., 2001. Experimental study of chaotic advection regime in a twisted duct flow. Eur. J. Mech. B 20, 205–232.
Lemenand, T., Peerhossaini, H., 2002. A thermal model for prediction of the Nusselt number in a pipe with chaotic flow. Appl. Therm. Eng. 22, 1717–1730.
Lemenand, T., Della Valle, D., Zellouf, Y., Peerhossaini, H., 2003. Droplet formation in turbulent mixing of two immiscible fluids in a new type of static mixer. Int. J. Multiphase Flow 29, 813–840.
Lemenand, T., Dupont, P., Della Valle, D., Peerhossaini, H., 2005. Turbulent mixing of two immiscible fluids. J. Fluids Eng. 127, 1132–1139.
Mokrani, A., Castelain, C., Peerhossaini, H., 1998a. Mesure du chaos dans les systèmes conservatifs en vue de l'étude des transferts dans les systèmes ouverts. Rev. General. Therm. 37, 459–474.
Mokrani, A., Castelain, C., Peerhossaini, H., 1998b. The effect of chaotic advection on heat transfer. Int. J. Heat Mass Transfer 40, 3089–3104.
Peerhossaini, H., Castelain, C., Le Guer, Y., 1993. Heat exchanger design based on chaotic advection. Exp. Therm. Fluid Sci. 7, 333–344.
Streiff, F.A., Mathys, P., Fischer, T.U., 1997. New fundamentals for liquid–liquid dispersion using static mixers. In: Recents Progrés en Genie des Procedés 11 (51, Mixing 97: Recent Advances in Mixing), pp. 307–314.
Taylor, G., 1953. Dispersion of soluble matter flowing slowly through a tube. Proc. Roy. Soc. Lond. A 219, 186–203.
Thakur, R.K., Vial, C., Nigam, K.D.P., Nauman, E.B., Djelveh, G., 2003. Static mixers in the process industries – a review. Inst. Chem. Eng. 81, 787–826.
Zhou, G., Kresta, S.M., 1998. Correlation of mean drop size and minimum drop size with the turbulence energy dissipation and the flow in an agitated tank. Chem. Eng. Sci. 53, 2063–2079.